

# Enhanced Grain Size and Crystallinity in $\text{CH}_3\text{NH}_3\text{PbI}_3$ Perovskite Films by Metal Additives to the Single-Step Solution Fabrication Process

Zahrah S. Almutawah, Suneth C. Waththage, Zhaoning Song, Ramez H. Ahangharnejhad, Kamala K. Subedi, Niraj Shrestha, Adam B. Phillips,\* Yanfa Yan, Randy J. Ellingson, and Michael J. Heben

Wright Center for Photovoltaics Innovation and Commercialization, School for Solar and Advanced Renewable Energy, Department of Physics and Astronomy, University of Toledo, Toledo, OH, USA 43606

## ABSTRACT

*Methods of obtaining large grain size and high crystallinity in absorber materials play an important role in fabrication of high-performance methylammonium lead iodide ( $\text{MAPbI}_3$ ) perovskite solar cells. Here we study the effect of adding small concentrations of  $\text{Cd}^{2+}$ ,  $\text{Zn}^{2+}$ , and  $\text{Fe}^{2+}$  salts to the perovskite precursor solution used in the single-step solution fabrication process. Enhanced grain size and crystallinity in  $\text{MAPbI}_3$  films were obtained by using 0.1% of  $\text{Cd}^{2+}$  or  $\text{Zn}^{2+}$  in the precursor solution. Consequently, solar cells constructed with Cd- and Zn-doped perovskite films show a significant improvement in device performance. These results suggest that the process may be an effective and facile method to fabricate high-efficiency perovskite photovoltaic devices.*

## INTRODUCTION

Organic-inorganic metal halide (OIMH) perovskite absorbers such as methylammonium lead iodide ( $\text{CH}_3\text{NH}_3\text{PbI}_3$ ,  $\text{MAPbI}_3$ ) have been used to prepare high-efficiency solar cells when they are paired with appropriate electron and hole transport layers (ETLs and HTLs). The power conversion efficiency (PCE) of OIMH perovskites solar cells has improved to ~23% [1]. The tremendous progress in improving PCE is mainly due to a unique combination of the intrinsic optical and electrical properties of OIMH perovskites, such as high absorption coefficients, long carrier diffusion lengths, desirable optical band gaps, fast carrier collection rates [2], and the existence of cost-effective and facile preparation methods [3]. Among several deposition methods, the single-step solution deposition coupled with the anti-solvent dropping technique has been widely used in the fabrication of high-efficiency perovskite solar cells [4]. Although, this method produces a dense, uniform, and conformal perovskite film, the size of the grains is relatively small (~200 nm). The small grains form a large number of grain boundaries that increases the density of charge carrier traps resulting in higher non-radiative recombination of carriers. By fabricating larger grains with a high degree of crystallinity, the non-radiative recombination in perovskite films can be reduced, and device performance improved [5-7].

Here, we adapt a technique demonstrated for the two-step deposition process [8] to enhance the grain size and crystallinity by adding small amounts of metal cations ( $\text{Cd}^{2+}$ ,  $\text{Zn}^{2+}$ , and  $\text{Fe}^{2+}$ ) during the single-step solution deposition process. This metal-additive-assisted single-step deposition fabrication process resulted in grains that are ~1  $\mu\text{m}$  in diameter, which is an increase of a factor of 5. In addition to the improved grain size, the degree of crystallinity of the grains and their optical properties are also improved with the metal cation inclusion, as determined by the X-ray diffraction (XRD) and photoluminescence (PL) analyses. With appropriate control of metal doping concentration, the PCE of perovskite solar cells was enhanced relative to devices constructed without metal addition.

## EXPERIMENTAL DETAILS

Fluorine-doped tin oxide (FTO) coated glass substrates (TEC 15, Pilkington NA) were cleaned in an ultrasonic bath using diluted Micro-90 detergent and deionized water. The samples were then rinsed with deionized water and thoroughly dried using nitrogen gas. A 50 nm SnO<sub>2</sub> ESL was prepared by spinning a stock solution of 15% SnO<sub>2</sub> colloidal dispersion in water (Alfa Aesar) diluted by H<sub>2</sub>O to 2.67% [9]. The deposited layer was dried at 150 °C for 30 min. The perovskite layer was prepared using the antisolvent-assisted single-step spin coating method [10]. A precursor solution consisting of 461 mg PbI<sub>2</sub> (Sigma Aldrich) and 159 mg methylammonium iodide (Sigma Aldrich) dissolved in a mixture of 78 mg dimethyl sulfoxide (DMSO) and 600 mg N,N-dimethylformamide (DMF) was spin-coated on the FTO/SnO<sub>2</sub> substrate first at 1000 rpm for 5 s, then at 4000 rpm for 25 s. The anti-solvent agent 0.55 ml diethyl ether was dripped on the rotating substrate at the 8th second of the second step. The as-deposited perovskite film was then annealed in air at 100 °C for 6 min. For the perovskite films with metal additives, small amounts (0.1% or 1% molar ratio) of CdCl<sub>2</sub>, ZnCl<sub>2</sub>, or FeCl<sub>2</sub> were added to the perovskite precursor solution. The HSL was prepared by spin coating the 2,2',7,7'-tetrakis(N,N-bis(p-methoxy-phenyl)amino)-9,9'-spirobifluorene (spiro-OMeTAD) following the process described in our earlier work [8]. Finally, a 40 nm Au electrode was evaporated via a shadow mask.

XRD spectra were obtained using a Rigaku Ultima III diffractometer. Scanning electron microscopy (SEM) images were taken using a field emission scanning electron microscope (Hitachi S-4800). The absorbance spectra were recorded using a spectrophotometer (Perkin Elmer Lambda 1050). PL measurements were performed with a 532 nm CW laser (beam diameter ~100 μm) at 94 mW/cm<sup>2</sup>. Samples were excited through film side. The PL signal was detected by a Horiba Symphony-II CCD detector (integration time = 0.5 s) after a 300 g/mm grating monochromator. PL spectra were obtained at several locations on the perovskite samples. Current density-voltage (J-V) curves were measured under simulated AM1.5G solar irradiation (Newport model 91195A-1000) using a Keithley 2400 source meter. The light intensity of the simulator was calibrated using a standard Si solar cell.

## RESULTS AND DISCUSSION

Figure 1 compares the SEM images of MAPbI<sub>3</sub> films formed from precursor solutions without and with divalent metal additives, including Cd<sup>2+</sup>, Zn<sup>2+</sup>, and Fe<sup>2+</sup>, at 0.1 and 1% molar ratios. All the samples show a dense and conformal surface morphology. However, the effect on the perovskite grain growth depends on the divalent metal cation used and its concentration. The grain size of the control sample is ~200 nm (Figure 1a), which is a typical value for perovskite films prepared by the single-step antisolvent method [10]. The inclusion of 0.1 and 1% Cd<sup>2+</sup> salts increased the grain size to ~600 nm (Figure 1b) and > 1 μm (Figure 1e), respectively. Interestingly, the impact of Zn<sup>2+</sup> incorporation is not monotonic. The inclusion of 0.1% Zn<sup>2+</sup> increased grain size to ~600 nm (Figure 1c); however, when the Zn<sup>2+</sup> concentration was increased to 1%, the grain size was ~350 nm (Figure 1f). In contrast to Cd<sup>2+</sup> and Zn<sup>2+</sup>, the addition of Fe<sup>2+</sup> has an adverse effect on grain growth. With 0.1 and 1% Fe<sup>2+</sup> additives, the grain size was ~200nm and ~100 nm, respectively (Figure 1d, g).

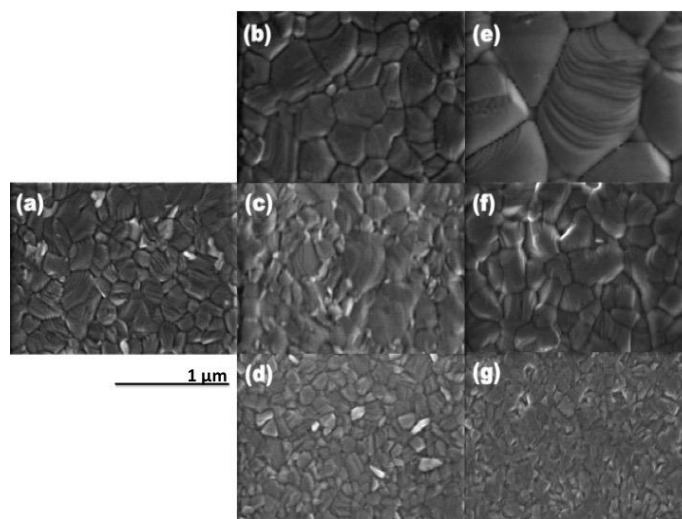


**Figure 1.** SEM images of MAPbI<sub>3</sub> films (a) without metal additives and with 0.1% (b) Cd<sup>2+</sup>, (c) Zn<sup>2+</sup>, and (d) Fe<sup>2+</sup>, and 1% (e) Cd<sup>2+</sup>, (f) Zn<sup>2+</sup>, and (g) Fe<sup>2+</sup>.

To further study the effects of metal additives on the crystallinity of perovskite films, we measured XRD spectra of the MAPbI<sub>3</sub> films without and with metal additives (Figure 2a, b). All perovskite films show characteristic XRD peaks for the tetragonal perovskite structure (space group I4/mcm) [11] with the most intense (110) peak located at ~14°. With the addition of divalent metal salts (Cd<sup>2+</sup>, Zn<sup>2+</sup>, and Fe<sup>2+</sup>) the (110) peak position shifted to higher values of 2θ (Figure 2c, d), indicating the incorporation of these metal additives into the perovskite crystal lattice. The partially substitution of Pb<sup>2+</sup> (ionic radii, R<sub>Pb2+</sub> = 133 pm) by cations with smaller sizes (R<sub>Cd2+</sub> = 109 pm, R<sub>Zn2+</sub> = 88 pm, and R<sub>Fe2+</sub> = 92 pm) [12] leads to the distortion and shrinkage of metal halide octahedra, and consequently, the shift of XRD peaks to higher angles. It is worth noting that for the 0.1% metal additive, the samples with Cd<sup>2+</sup> and Zn<sup>2+</sup> have a slightly lower full width-half max than control film, while this is only the case for Cd<sup>2+</sup> when 1% is used [13].

The intensity of the (110) XRD peak increased with the addition of 0.1% metal salts (Figure 2c), indicating a higher degree of crystallinity than the control sample. However, the (110) peak intensity decreased when the metal additive concentration was increased from 0.1 to 1% (Figure 2d). In contrast, the film with 1% Cd<sup>2+</sup> shows a higher intensity of the (110) peak and has a smaller peak width than the control sample, indicating a higher degree of crystallinity and larger grains.

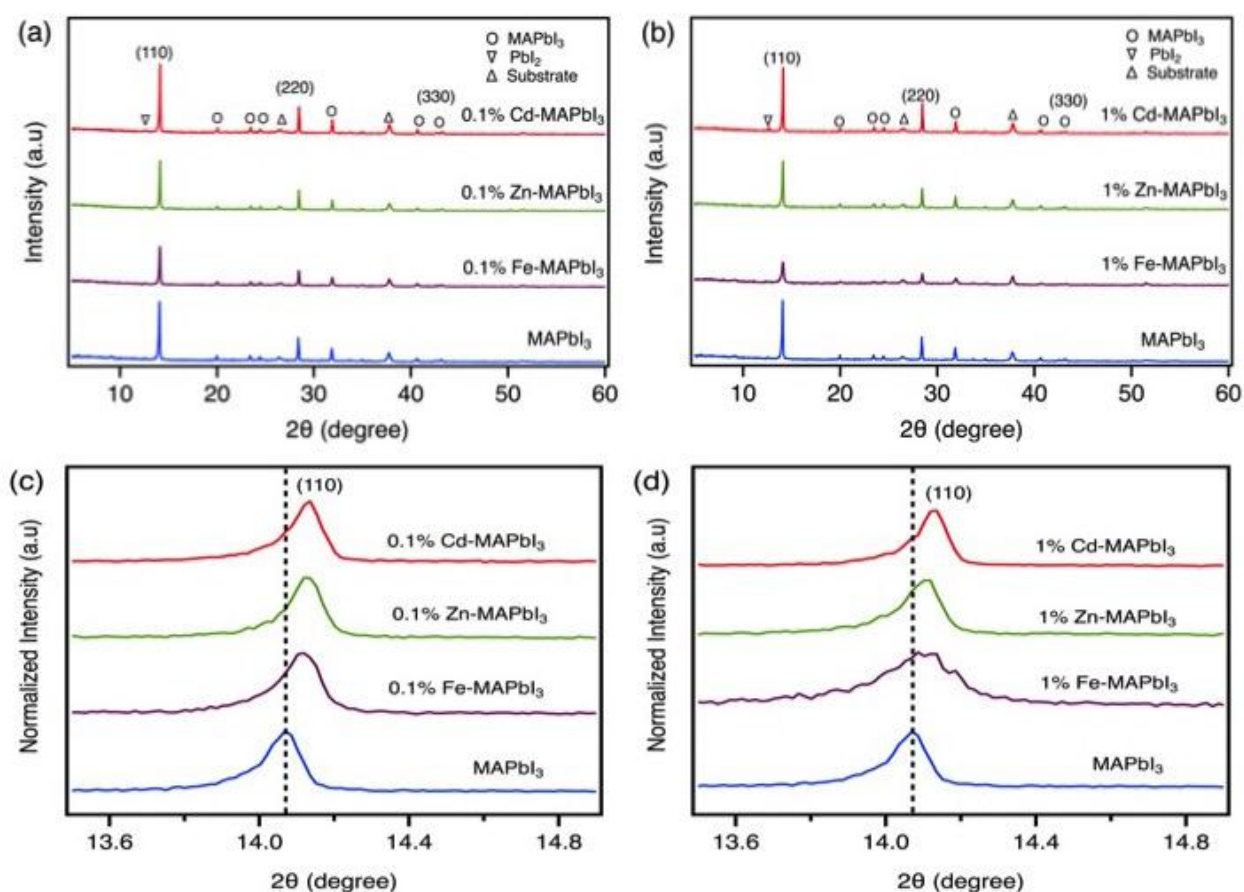


**Figure 2.** XRD spectra of MAPbI<sub>3</sub> thin films with (a) 0.1% and (b) 1% metal additives. Panels (c) and (d) are zoom-in of the normalized XRD spectra of the perovskite (110) peaks shown in (a) and (b) to better show the peak shift and shape.

Figure 3 shows the absorbance and PL spectra of the MAPbI<sub>3</sub> film without and with metal additives. All the films with metal additives show a strong optical absorption at the perovskite band edge of ~770 nm (Figure 3a, b), consistent with the PL emission from the MAPbI<sub>3</sub> perovskite centered at 768 nm (Figure 3c, d). The PL intensities of films with 0.1% Zn and Cd addition are higher than that of the control sample (Figure 3c), consistent with larger grain size and better crystallinity. In contrast, the inclusion of Fe<sup>2+</sup> significantly decreased the PL intensity, indicating the formation of non-radiative recombination centers. This could be due to the introduction of traps for mobile charge carriers from the multivalent states of Fe (2+/3+) [14]. The films with 1% Cd<sup>2+</sup> and Zn<sup>2+</sup> show a widening and small shift of the PL emission peak. In the case of Cd addition, a blue-shift in the PL emission peak is observed, which could be related to a

lattice contraction due to  $\text{Pb}^{2+}$  substitution by  $\text{Cd}^{2+}$  [13]. This, though, is inconsistent with the XRD data, which shows no difference in peak location between the 0.1% and 1%  $\text{Cd}^{2+}$  films. It is not clear why this shift is occurring. In contrast, the addition of 1%  $\text{Zn}^{2+}$  leads to a red-shift in the PL emission peak. Because the size of  $\text{Zn}^{2+}$  is much smaller than  $\text{Pb}^{2+}$ ,  $\text{Zn}^{2+}$  ions may not form the substitutional defects but exits as interstitial defects or segregate as metal complexes on the grain boundaries, introducing shallow defects levels that cause PL peak shift towards a lower energy. These peak shifts are not observed in samples with 0.1% metal additives because of the low concentration of dopants. No PL signals were observed from the film with 1%  $\text{Fe}^{2+}$ , which confirms that Fe (2+/3+) impurities are detrimental to the perovskite optoelectrical properties.

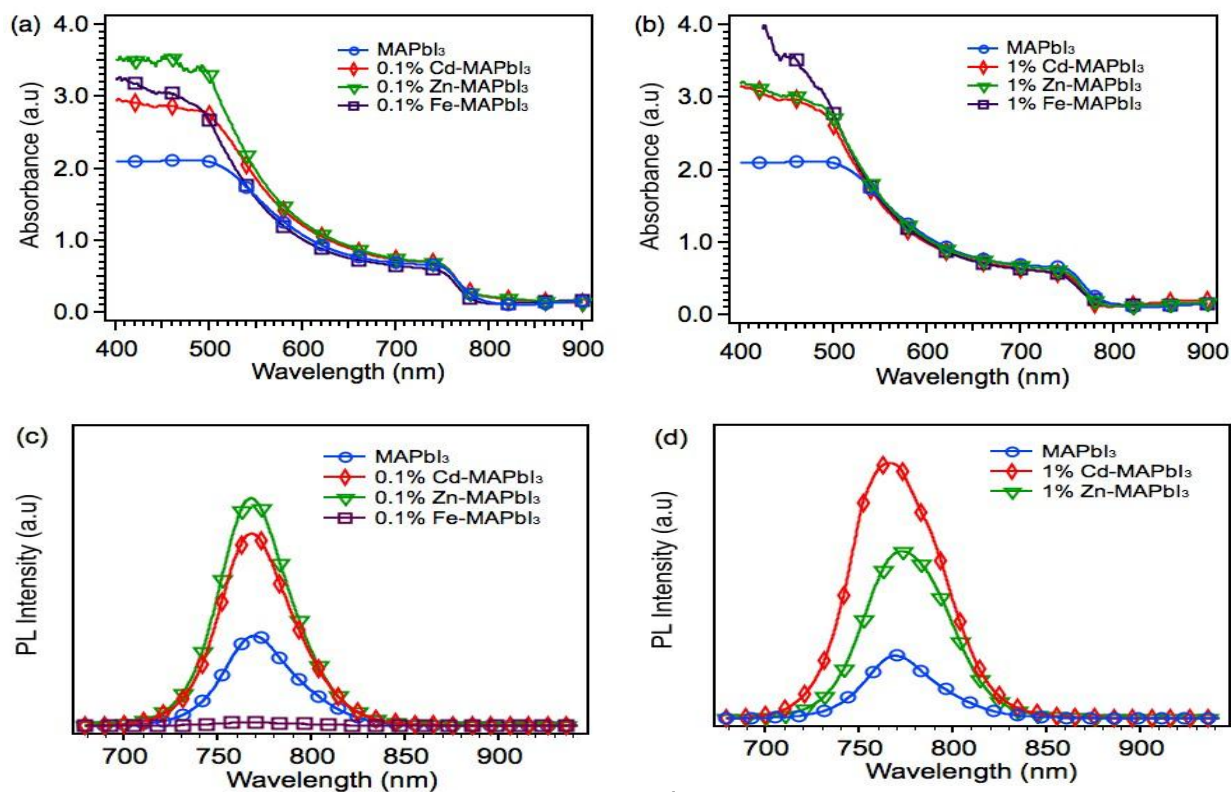


**Figure 3.** Absorbance spectra of  $\text{MAPbI}_3$  thin films with (a) 0.1% and (b) 1% metal additives. PL spectra of  $\text{MAPbI}_3$  films with (c) 0.1% and (d) 1% metal additives.

The SEM images and XRD and PL spectra show that including small amounts of  $\text{Cd}^{2+}$  and  $\text{Zn}^{2+}$  in the fabrication process improves the crystallinity of the films and that this improvement is not monotonic with increasing metal concentration. Clearly these additives are affecting the nucleation and growth of the perovskite films. We showed that the addition of  $\text{Cd}^{2+}$  in the two-step process resulted in Cd-containing low dimensional perovskites (LDPs) forming between the MAI and Cd [8]. In that case, the terraced edges of the  $\text{PbI}_2$  are the energetically preferred location for the Cd-LDPs, so incorporation of MAI into the  $\text{PbI}_2$  lattice occurs without an energy barrier. In the one-step process, though, the crystallites are formed in the mixed perovskite precursor solution and the second solvent, in our case DMSO, inhibits growth [15]. The SEM images of the as-deposited perovskite films, Figure 4, show that the grain size is the same without and with  $\text{Cd}^{2+}$ . This indicates that the presence of DMSO restricts the growth mechanism. It is likely that Cd-LDPs are formed at the edges of the crystallites. Upon removal of the DMSO through heating, the grain growth is similar to the Cd-assisted grain growth in the two-step process, where the Cd-LDPs enable the Volmer-Weber type growth.  $\text{Zn}^{2+}$  acts similar to  $\text{Cd}^{2+}$  but appears to saturate below 1%. In contrast,  $\text{Fe}^{2+}$  do not form LDP phases which are compatible with  $\text{MAPbI}_3$  so that the effect on grain growth is negligible.

To investigate the impact of the enhanced grain size and crystallinity in  $\text{MAPbI}_3$  films on the photovoltaic device performance, we fabricated perovskite solar cells in the FTO/ $\text{SnO}_2$ / $\text{MAPbI}_3$ /Spiro-OMeTAD/Au configuration. J–V curves of the best performing devices based on the  $\text{MAPbI}_3$  films without and with metal additives are shown in Figure 5. The solar cell performance metrics for these devices are tabulated in Table I. When measured in the reverse direction (from forward to reverse bias), the control device has a short-circuit current density ( $J_{\text{sc}}$ ) of  $17.5 \text{ mA/cm}^2$ , an open-circuit

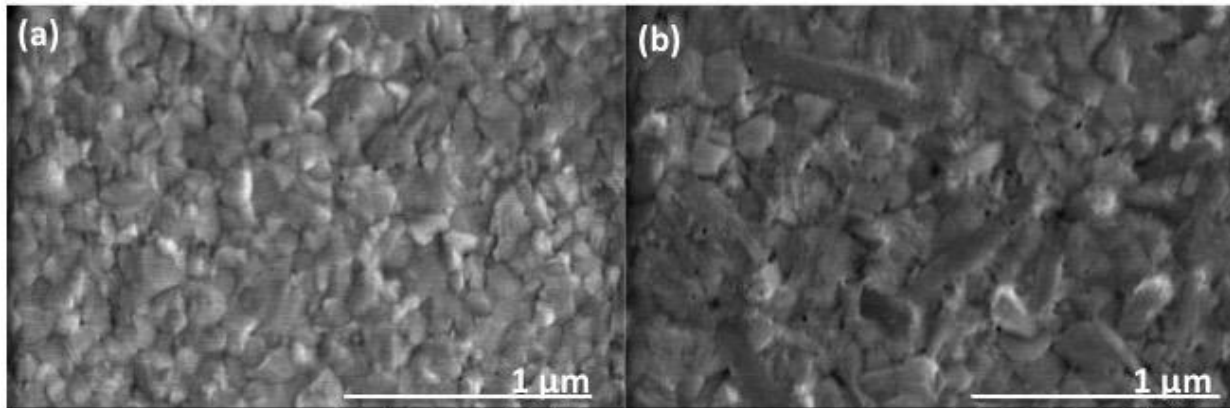


**Figure 4.** SEM images of the surface of MAPbI<sub>3</sub> thin films prepared before heating (a) without additive (b) with 1% Cd<sup>2+</sup>.

voltage ( $V_{OC}$ ) of 1.0 V, and a fill factor (FF) of 66.20%, yielding a PCE of 11.7%. With 0.1% Cd<sup>2+</sup>,  $J_{SC}$ ,  $V_{OC}$ , FF, and PCE increased to 18.7 mA/cm<sup>2</sup>, 1.0 V, 67.304%, and 12.8%, respectively. The device based on the perovskite film with 0.1% Zn<sup>2+</sup> shows a significant improvement on all the metrics, yielding  $J_{SC} = 19.30$  mA/cm<sup>2</sup>,  $V_{OC} = 1.04$  V, FF = 68.6%, and PCE = 13.76%. This improvement due to addition of Zn<sup>2+</sup> is consistent with a previous report that demonstrated a superior solar cell performance of Zn-doped perovskite [16]. As expected, the devices with Fe<sup>2+</sup> additives show poor performance because of the non-radiative defects introduced by the Fe-based impurities. Increasing the metal salt concentrations from 0.1 to 1% leads to a decline in the device performance for all three metal additives. Therefore, the optimal additive concentration should lie between 0.1 to 1%, and further work is needed to determine the best doping concentration. All our devices demonstrate significant hysteresis, likely due to the unbalanced charge collections at the MAPbI<sub>3</sub>/SnO<sub>2</sub> and MAPbI<sub>3</sub>/Spiro-OMeTAD interfaces. The hysteresis could be remedied by introducing an interface layer with better condition band alignment with the perovskite, such as C60-SAM. The hysteresis, though, does not appear to be affected by the metal additive.

## CONCLUSION

We have shown that the addition of appropriate amounts of Cd and Zn salts into perovskite precursor solution can significantly enhance grain size and crystallinity of the MAPbI<sub>3</sub> films prepared by the single-step solution method. The increased grain size and crystallinity increases the PL response of the films as the number of nonradiative recombination sites at the grain boundaries and inside the grain decrease. This leads to improved solar cell performance.

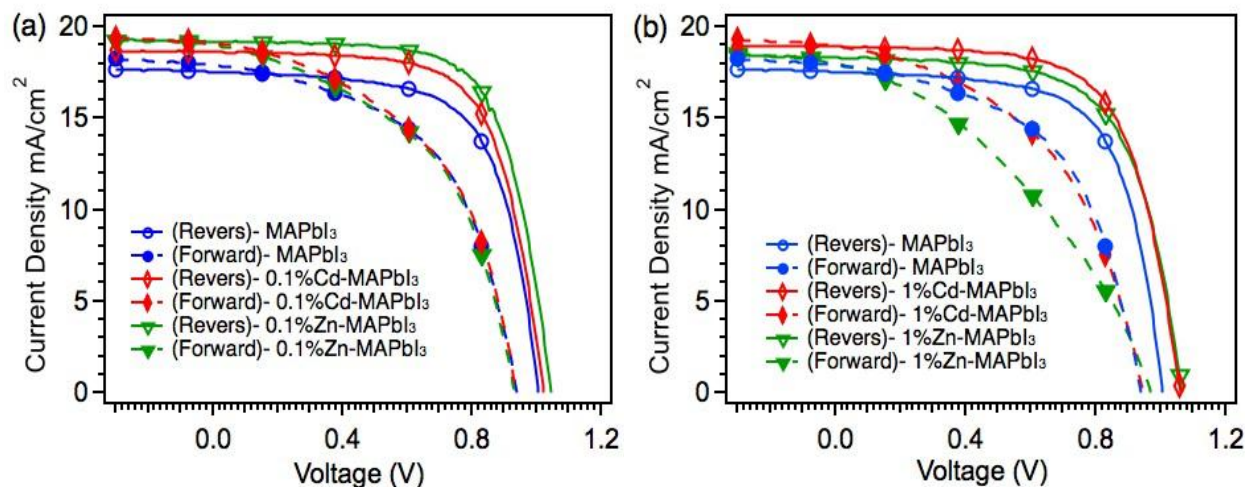


**Figure 5.** J-V curves of perovskite solar cells based on MAPbI<sub>3</sub> with (a) 0.1% and (b) 1% metal additives.

Table I. Solar cell performance metric for MAPbI<sub>3</sub> solar cells with metal additives

Absorber	Scan	J <sub>SC</sub> (mA/cm <sup>2</sup> )	V <sub>OC</sub> (V)	FF (%)	PCE (%)
MAPbI <sub>3</sub>	Reverse	17.5	1.0	66.2	11.7
	Forward	17.9	0.94	53.2	8.96
0.1% Cd	Reverse	18.7	1.0	67.3	12.8
	Forward	19.0	0.9	49.8	8.9
0.1% Zn	Reverse	19.2	1.05	68.6	13.76
	Forward	19.0	0.93	49.6	8.8
1% Cd	Reverse	18.9	1.1	65.9	13.2
	Forward	18.9	0.95	48.2	8.7
1% Zn	Reverse	18.3	1.1	64.9	12.7
	Forward	17.99	0.97	37.5	6.55

## ACKNOWLEDGMENTS

This work was financially supported by the Air Force Research Laboratory, Space Vehicles Directorate (contract no. FA9453-11-C-0253), Office of Naval Research (contract no. N00014-17-1-2223) and the National Science Foundation (contract no. ECCS-1665172).

## REFERENCES

1. NREL. *Solar Cell Efficiency Chart*. Available from: <https://http://www.nrel.gov/pv/assets/images/efficiency-chart.png> (accessed 18 March 2018).
2. Correa-Baena, J.-P., et al., *Promises and challenges of perovskite solar cells*. *Science*, 2017. **358**(6364): p. 739-744.
3. Song, Z., et al., *A technoeconomic analysis of perovskite solar module manufacturing with low-cost materials and techniques*. *Energy & Environmental Science*, 2017. **10**: p. 1297-1305.
4. Song, Z., et al., *Pathways toward high-performance perovskite solar cells: review of recent advances in organo-metal halide perovskites for photovoltaic applications*. *Journal of Photonics for Energy*, 2016. **6**(2): p. 022001.
5. Nie, W., et al., *High-efficiency solution-processed perovskite solar cells with millimeter-scale grains*. *Science*, 2015. **347**(6221): p. 522-525.
6. Bi, C., et al., *Non-wetting surface-driven high-aspect-ratio crystalline grain growth for efficient hybrid perovskite solar cells*. *Nature Communications*, 2015. **6**: p. 7747.
7. Tress, W., et al., *Interpretation and evolution of open-circuit voltage, recombination, ideality factor and subgap defect states during reversible light-soaking and irreversible degradation of perovskite solar cells*. *Energy & Environmental Science*, 2018. **11**(1): p. 151-165.
8. Wathage, S.C., et al., *Enhanced Grain Size, Photoluminescence, and Photoconversion Efficiency with Cadmium Addition during the Two-Step Growth of CH<sub>3</sub>NH<sub>3</sub>PbI<sub>3</sub>*. *Acs Applied Materials & Interfaces*, 2017. **9**(3): p. 2334-2341.
9. Jiang, Q., et al., *Enhanced electron extraction using SnO<sub>2</sub> for high-efficiency planar-structure HC(NH<sub>2</sub>)<sub>2</sub>PbI<sub>3</sub>-based perovskite solar cells*. *Nature Energy*, 2016. **2**: p. 16177.
10. Ahn, N., et al., *Highly Reproducible Perovskite Solar Cells with Average Efficiency of 18.3% and Best Efficiency of 19.7% Fabricated via Lewis Base Adduct of Lead(II) Iodide*. *Journal of the American Chemical Society*, 2015. **137**(27): p. 8696-8699.
11. Song, Z., et al., *Impact of Processing Temperature and Composition on the Formation of Methylammonium Lead Iodide Perovskites*. *Chemistry of Materials*, 2015. **27**(13): p. 4612-4619.
12. *Radii of atoms and ions*. Available from: [https://http://www.webelements.com/zinc/atom\\_sizes.html](https://http://www.webelements.com/zinc/atom_sizes.html) (accessed 14 April 2018).
13. Wathage, S.C., et al., *Impact of Divalent Metal Additives on the Structural and Optoelectronic Properties of CH<sub>3</sub>NH<sub>3</sub>PbI<sub>3</sub> Perovskite Prepared by the Two-Step Solution Process*. *MRS Advances*, 2017: p. 1-6.
14. Frolova, L.A., et al., *Exploring the Effects of the Pb<sup>2+</sup> Substitution in MAPbI<sub>3</sub> on the Photovoltaic Performance of the Hybrid Perovskite Solar Cells*. *The Journal of Physical Chemistry Letters*, 2016. **7**(21): p. 4353-4357.
15. Benjamin, J.e.a., *Controlling nucleation, growth, and orientation of metal halide perovskite thin films with rationally selected additives*. *Materials Chemistry A*, 2017. **5**(2050-7488): p. 113.
16. Zhao, W., et al., *Zn-doping for reduced hysteresis and improved performance of methylammonium lead iodide perovskite hybrid solar cells*. *Materials Today Energy*, 2017. **5**: p. 205-213.